ELSEVIER

Journal of Materials Processing Technology 114 (2001) 1–17

Journal of Materials Processing Technology

www.elsevier.com/locate/jmatprotec

Semi-empirical model on work removal and tool wear in electrical discharge machining

Pei-Jen Wang, Kuo-Ming Tsai*

Department of Power Mechanical Engineering, National Tsing Hua University, 101, Sec 2, Kuang Fu Road, Hsinchu 30043, Taiwan, ROC

Received 3 June 1999

Abstract

A semi-empirical model of the material removal rate on the work and the tool for various materials has been established by employing dimensional analysis based upon pertinent process parameters screened by the design of experiment in the electrical discharge machining process. The parameters of the model, such as the peak current, pulse duration, electric polarity, and the properties of materials, have been systematically selected and then verified by making use of the standard Taguchi method. Predictions based on the semi-empirical model with model parameters being calculated by a non-linear optimization method have shown a good agreement with the experimental verifications. © 2001 Published by Elsevier Science B.V.

Keywords: Electrical discharge machining; Semi-empirical model

1. Introduction

Electrical discharge machining (EDM) is classified as a non-traditional machining process for metal removing based on the feature that no tool force is generated during machining. The removal of metals in the EDM process is associated with the erosive effects occurring under a series of successive electrical sparks generating between the tool and the workpiece submerged in a dielectric liquid environment. The EDM process is widely used for machining high strength steel, tungsten carbides and hardened alloy steel, which are difficult to cut by the traditional machining process in the manufacturing of tools, dies and molds. The material removal mechanism of the EDM process is primarily based on a thermal conduction phenomenon governed by the thermal energy generated from an arc channel and quickly dissipated into the electrode and the work. As a result, the work material near the discharge location is melted, vaporized and then flushed off by the dielectric liquid. It is evident that there are many process variables that affect the material removal rate (MRR) on the work in the EDM process. From the observations in previous publications, the most important variables are level of peak current, the duration of the current pulse, the open voltage of the gap, the polarity of the electrode, the thermodynamic properties of the tool and the work, and the physical properties of the tool and the work.

From the literature, there are basically two approaches, either the theoretical or the empirical, in the study of the EDM process. The theoretical work is based on solid-state physics, thermodynamics and electrodynamics; and the goal is to describe the physical behavior by making use of a physical model [1–4]. Certainly, researchers have encountered major difficulties due to the complexity of the physics. The inevitable assumptions and simplified approaches push the physical model far away from reality. On the other hand, experimentalists have tried to establish empirical models based on statistical analysis and optimization methods. Various empirical models for MRR on the work or tool have been published in the past [5–10]. Longfellow et al. [5] proposed an empirical model on the tool wear ratio based on the cohesive energy of the work and the tool. Greene and Guerrero-Alvarez [6] reported that the volume eroded from the tool depends on the cohesive energy and the melting point of the tool. Jeswani [7] showed that the above models have a poor fit between experimental values and the predictions of the wear ratio. In his paper, the measured wear ratios on silver and copper for the tool, and iron for the work, were compared with the predicted wear ratios, and were about one order of magnitude difference, which indicates

* Corresponding author. Fax: +886-3-572-2840.
E-mail address: tsai101@chinyi.ncit.edu.tw (K.-M. Tsai).

0924-0136/01/$ – see front matter © 2001 Published by Elsevier Science B.V.
PII: S0924-0136(01)00733-6

that the cohesive energy is not the only property that influences the wear ratio. In addition, he derived a model for tool wear based on dimensional analysis. The model included various properties of the materials and the discharge pulse energy that are difficult to be measured in practice. In 1982, Osyczka et al. [8] showed four models specifically on metal removal rate, tool wear, surface roughness, and power consumption by employing identification and multi-criterion optimization methods. The four models considered both process conditions and the final geometry of the work. There were also models on the MRR of the tool based on the peak current and pulse duration [9,10], but these specific models were only valid for the selected tool and work with fixed electric polarity. By assuming that the properties of the tool and the work are irrelevant, the models showed a large discrepancy between the predictions and the experimental results.

It might be noted that although an enormous amount of research effort has been put in to represent the EDM process by empirical models, a more elaborate semi-empirical model based not only on thermal–mechanical but also statistical approaches has not yet been reported. The objective of this paper is to develop a semi-empirical model on the MRR of the work and the tool for various materials. The following study was to identify the level of importance of the process parameters from pre-selected six process parameters, namely peak current, gap open-voltage, pulse on-time, pause time, servo voltage, and electric polarity, for various tools and work by screening experiments. All the experiments were carefully conducted by employing the design of experiment (DOE) technique, namely the standard Taguchi method [11,12]. Details of the DOE theory, published in some textbooks, are not described in this paper. Finally, the response surface technique [13] was used for verification for the screening experiments. Then, a general (MRR model based on dimensional analysis of pertinent process variables was obtained and the coefficients of the model were calculated by making use of various optimization methods.

2. Experimental procedure

2.1. Experimental apparatus

A CNC electric discharge machine, Model Mold Maker 3 made by Sodick in Japan was used for the experiments. The machine was attached to a MARK XI Pulse-charge Generator and associated controller to produce rectangular-shaped current pulses for discharging purpose. The level of discharge current was measured with a Hall-effect current sensor, Model HNC-200P made by Nana Electronics in Japan, which has built-in voltage amplifier for amplifying the current pulses to appropriate voltage levels. Both the voltage and the current waveform on the tool were measured with a digital storage oscilloscope. By looking into the environmental effects, the temperature of the work and the dielectric fluid was monitored by PT-100 temperature probes. Concerning data analysis, an ACL-8112HG data acquisition card attached to a personal computer was used for sampling the essential signals for all experiments. In order to be able to control the environment, the dielectric fluid was confined within a stainless steel container throughout the experiments. A schematic drawing and a photograph of the experimental system is shown in Fig. 1 in which the tool is shown at the upper electrode position and the work is shown at the lower table position.

For the DOE data analysis, a statistical software package S-PLUS with DOX module, copyrighted by Statistical Sciences, USA, was used to analyze the data [14]. As for data fitting of the model coefficients, the MATLAB with Optimization Toolbox [15], copyrighted by the MathWork, USA, was employed for optimizing the non-linear equations.

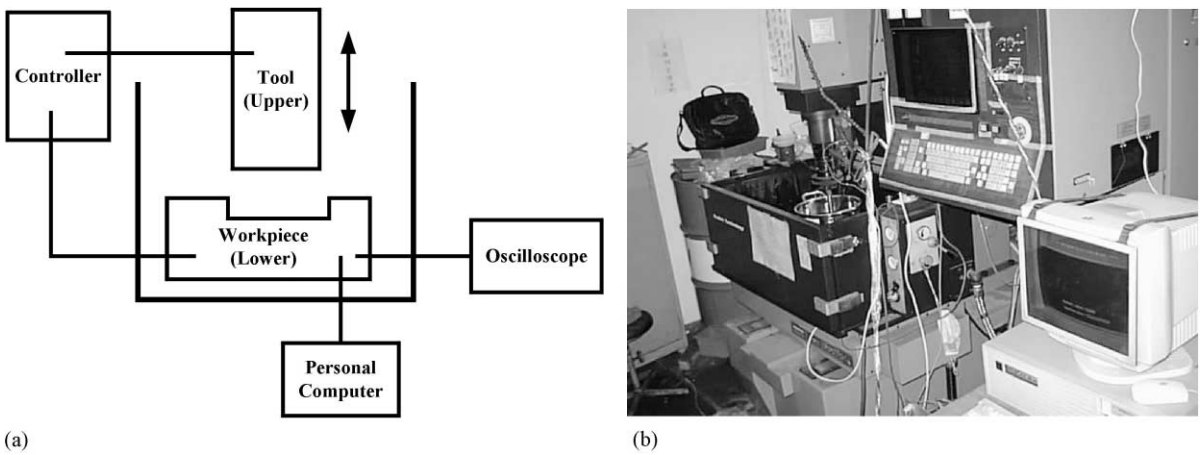

Fig. 1. Showing: (a) a schematic drawing and (b) a photograph of the experimental system.

Table 1
Experimental materials for the screening experiments

Materials	Composition	Hardness	Density (kg/m^3)	Machined roughness R_{max} (μm)	Dimension $\phi \times l$ (mm)
Tool					
Cu	>99.95%	HRB 55	8896.6	4.02	9.5×50
Gr(ISEM-8)	*g*-factor 64–70	65 (shore)	1754.5	18.935	10×60
Ag–W	W 70%, Ag 30%	HRB 85	14904.7	3.5	10×60
Work					
AISI EK2	C 1.19%, Mn 0.35%, Cr 0.18%	HB179	7809.9	1.42	25×13
AISI D2	C 1.52%, Mn 0.34%, Cr 11.29%, Mo 0.71%, V 0.59%	HB217	7723.0	1.47	25×13
AISI H13	C 0.43%, Si 1.04%, Mn 0.33%, Mo 1.33%, V 0.98%	HB187	7737.4	1.275	25×13

Table 2
Parameters and levels for the screening experiments

Factors	Symbol	Parameters	Level		
			1	2	3
Control factor	A(PL)	Polarity of tool (upper)	−	+	
	B(ON)	Discharge time (μs)	30	60	120
	C(OFF)	Quiescent time (μs)	30	60	120
	D(I_p)	Peak current (A)	12	30	48
	E(SV)	Servo standard voltage	0	1	2
	F(V)	Main power voltage (V)	60	90	120
	G(An)	Tool materials (upper)	Cu	Gr	Ag–W
	H(Ca)	Work materials (lower)	EK2	D2	H13
Noise factor	Temp	Temperature of dielectric fluid (°C)	30	50	

2.2. Materials and designs

In this study, two levels of experimental work are needed to establish the semi-empirical model. The first step is to identify the pertinent process parameters by screening experiments. For convenience, three types of materials, namely copper, graphite, and silver–tungsten alloy, were used for the tool; while three grades of steel were used for the work. According to the DOE results, the pertinent parameters would be selected for establishing the model. Table 1 shows the pertinent characteristics and the dimensions of the tool and the work. Due to the limitations on the electrical and mechanical capacity of the EDM machine, preliminary tests were conducted for defining the proper range of the parameters and the levels listed with corresponding symbols in Table 2. Only eight parameters were selected and put into Table 2 because of their possible effects on the work.

After the importance level of the parameters had been determined, a dimensional equation could be formulated with the help of dimensional analysis. At this stage, the second step was to do more experiments for final verification on the semi-empirical model. It might be noted that pure metals were used for the tool and the work because they have traceable physical properties. Copper and silver were used for the tool, while aluminum, iron and titanium were used for the work.

The dimensions and pertinent thermal and physical properties of the metals are tabulated in Tables 3 and 4, respectively. The parameters and the levels for the verification experiments corresponding to Tables 3 and 4 are given in Table 5.

2.3. Screening procedure

The purpose of the screening experiment is to identify the process parameters that have the most important influence in the EDM process. Based on past experience, there are many parameters that affect the quality characteristics of the EDM process. In this paper, the standard Taguchi method was used to identify the significant parameters by screening experiments. Six process parameters plus the tool and the work materials were selected to make the eight controllable parameters in the inner array (i.e. control factors). The outer array (i.e. noise factors) was chosen to be the temperature of dielectric fluid. Therefore, the inner array is an $L_{18}(2^1 \cdot 3^7)$ array and the outer array is an $L_2(2^1)$ array. The $L_{18}(2^1 \cdot 3^7)$ array is for the study of the main effect of all control factors. The block diagram of the screening experiment procedure is shown in

Table 3
Characteristics and dimensions of experimental materials for verification experiment

Materials	Composition (%)	Density (kg/m^3)	Machined roughness R_{max} (μm)	Dimensions $\phi \times l$ (mm)
Tool				
Cu	>99.95	8896.6	4.02	9.5×50
Ag	>99.99	10490	5.41	10×60
Workpiece				
Fe	>99.9	7870	1.08	20×12
Al	>99.5	2699	2.76	20×12
Ti	>99.9	4507	4.325	25×13

Table 4
Thermal and physical properties of the materials given in Table 3

Thermal and physical properties	Unit	Cu	Ag	Al	Fe	Ti	Reference
Density	g/cm^3	8.96	10.5	2.70	7.86	4.51	[16]
Electrical conductivity	$\times 1\ 0^{\ 5}$ $(\Omega\,\mathrm{cm})^{-1}$	5.88	6.21	3.65	1.02	0.23	[17]
First ionization energy (remove one electron)	eV[a]	7.724	7.574	5.984	7.87	6.82	[17]
	kcal/g[b]	(178)	(175)	(138)	(182)	(158)	
Cathode fall	eV	14.7–15.4	12.1–13.6	17.2–18.6	17.1–18.0	16.8–17.6	[18,19]
	eV (air)[c]	(8–12)			(8–12)		
	kcal/g	(346.8)	(296.1)	(412.5)	(404.4)	(396.4)	
Anode fall	eV	10					[19]
	eV (air)	(2–6)			(2–10)		
	kcal/g	(178)	(174.5)	(137.9)	(181.4)	(157.2)	
Work function	eV	4.47	4.28	3.74	4.36	4.09	[20,21]
	kcal/g	(103)	(98.6)	(66.2)	(100.5)	(94.3)	
Thermal conductivity	W/cm K	3.98	4.27	2.37	0.803	0.22	[22]
	cal/s cm K	0.95	1.020	0.566	0.192	0.055	
Specific heat	cal/g K	0.092	0.056	0.215	0.11	0.126	[22]
	cal/mol K	(5.846)	(6.041)	(5.801)	(6.143)	(6.035)	
Heat of fusion	kcal/mol	3.11	2.70	2.55	3.67	3.7	[20]
	kcal/g	(0.0489)	(0.025)	(0.0945)	(0.0657)	(0.0772)	
Heat of vaporization	kcal/mol	72.8	60.7	67.9	84.6	106.5	[20]
	kcal/g	(1.1456)	(0.5627)	(2.5165)	(1.5149)	(2.2233)	
Melting point	K	1356	1233.8	933	1809	1941	[16]
Boiling point	K	2868	2483	2723	3273	3533	[16]

[a] Ionization potential $\approx 2 \times$ work function.

[b] $1\,\mathrm{eV} = \dfrac{1.60219 \times 10^{-19}\,(\mathrm{J})}{1.6606 \times 10^{-24}\,(\mathrm{g})} \times \dfrac{1}{4.1868\,(\mathrm{J})} = 23.04447231\,(\mathrm{kcal/g})$.

[c] Anode fall $\approx$ ionization potential for gas discharge.

Table 5
Parameters and levels for verification experiment on semi-empirical model

Symbol	Parameter	Level				
		1	2	3	4	5
PL	Polarity of upper electrode	−	+			
ON	Discharge time (μs)	20	30	60	100	
I_p	Main power peak current (A)	12	22.5	30	39	48
An	Tool material (upper electrode)	Cu	Ag			
Ca	Work material (lower electrode)	Al	Fe	Ti		
OFF	Quiescent time (μs)	60				
V	Main power voltage (V)	90				
SV	Servo standard voltage	2				

Table 6
Experimental results of screening experiments based on DOE

Experiment No.	Control factor								MRR of workpiece (mm^3/min)		Tool wear (mm^3/min)		S/N (dB)	
	A(PL)	B(ON)	C(OFF)	D(I_p)	E(SV)	F(V)	G(An)	H(Ca)	Temp−	Temp+	Temp−	Temp+	MRR of workpiece, $\hat{\eta}_L$	Tool wear, $\hat{\eta}_S$
1	1	1	1	1	1	1	1	1	0.0218	0.1063	0.01349	0.0742	−30.41	25.46
2	1	1	2	2	2	2	2	2	16.7706	16.6308	3.1007	3.3515	24.45	−10.18
3	1	1	3	3	3	3	3	3	0.3567	0.2843	0.0530	0.0503	−10.05	25.74
4	1	2	1	1	2	2	3	3	0.1086	0.0737	0.0389	0.0275	−21.29	29.45
5	1	2	2	2	3	3	1	1	0.7785	0.7478	0.2675	0.2597	−2.35	11.58
6	1	2	3	3	1	1	2	2	18.5886	18.2571	3.0950	3.1406	25.31	−9.88
7	1	3	1	2	1	3	2	3	2.8976	2.8588	0.8493	0.7467	9.18	1.94
8	1	3	2	3	2	1	3	1	1.4277	1.3163	0.1369	0.1382	2.73	17.23
9	1	3	3	1	3	2	1	2	0.0647	0.0596	0.0090	0.0202	−24.15	36.12
10	2	1	1	3	3	2	2	1	17.6083	18.0782	1.3110	1.2939	25.03	−2.30
11	2	1	2	1	1	3	3	2	0.8727	0.9530	0.0463	0.0436	−0.82	26.94
12	2	1	3	2	2	1	1	3	1.1360	1.2097	0.5317	0.5530	1.37	5.31
13	2	2	1	2	3	1	3	2	10.9025	11.0436	0.3274	0.3361	20.81	9.58
14	2	2	2	3	1	2	1	3	5.8159	6.0576	1.5680	1.6433	15.47	−4.12
15	2	2	3	1	2	3	2	1	2.0820	2.0371	0.2565	0.2622	6.27	11.72
16	2	3	1	3	2	3	1	2	29.7030	28.4254	0.4541	0.4507	29.26	6.89
17	2	3	2	1	3	1	2	3	0.3877	0.4317	0.0912	0.0798	−7.79	21.34
18	2	3	3	2	1	2	3	1	3.8016	3.8720	0.0738	0.0751	11.68	22.56
Average									6.30	6.25	0.6791	0.6970	4.150	12.52
Total average									6.271		0.6881			

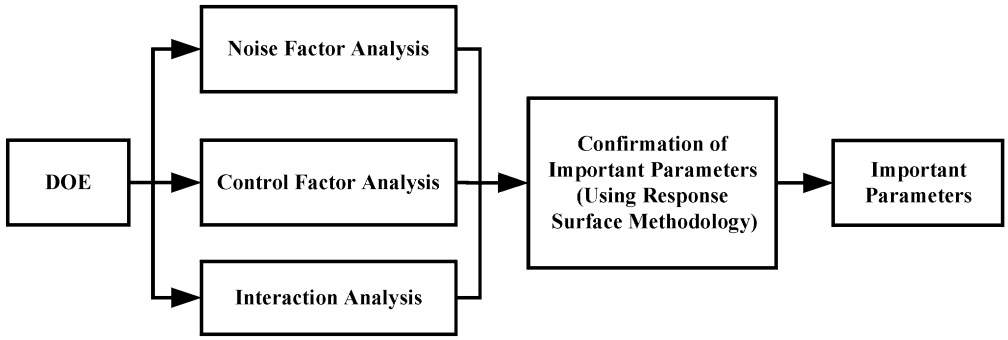

Fig. 2. Procedure diagram of the screening experiment.

Fig. 2 where the effects of noise factor, control factor and interactions between control factors must be completely analyzed individually. After confirmation of the parameters, the important parameters in the EDM process could then be obtained.

It is a common practice that the Taguchi method requires both analysis of the mean response for each run in the inner array and analysis of variations by using appropriately chosen signal to noise ratios (S/N ratio) derived from a quadratic loss function. In the EDM process, the MRR of the work is a larger-the-better (LTB) quality characteristic; and the tool wear is a smaller-the-better (STB) quality characteristic.

The S/N equation for the larger-the-better quality characteristic is defined as

$$\hat{\eta}_{\mathrm{L}} = -10\log\left[\frac{1}{n}\sum_{i=1}^{n}\frac{1}{y_i^2}\right](\mathrm{dB}) \tag{1}$$

and the S/N equation for the smaller-the-better quality characteristic is defined as

$$\hat{\eta}_{\mathrm{S}} = -10\log\left[\frac{1}{n}\sum_{i=1}^{n}y_i^2\right](\mathrm{dB}). \tag{2}$$

The experimental results of the screening experiment are tabulated in Table 6. One might just need to both maximize the MRR of work and minimize the tool wear by the S/N values.

2.4. Noise factor analysis

The comparison on the effects of the noise factor, namely the temperature of the dielectric fluid, in the EDM process are illustrated in Table 7. The results indicate that almost no difference exists between the levels of the noise factor for both the MRR of the work and the tool. Therefore, it is concluded that the effects of temperature of the dielectric fluid within the selected temperature range are negligible. The rationale is that the temperature rise of the dielectric fluid is much lower than the temperature rise in the discharge channel.

Table 7
Mean response of the noise factor

Level (°C)	MRR of work (mm^3/min)	Tool wear (mm^3/min)
30	6.30	0.6791
50	6.25	0.6970
$\lvert\Delta\rvert$	0.05	0.0179

2.5. Control factor analysis

A first-order linear contrast is usually employed for analyzing the linear relationship of the performances and the factors. Similarly, a second-order quadratic contrast can be used to analyze the non-linear relationship of the performances and the factors as described in Montgomery's book [11]. With the help of S-PLUS, the Pareto plots of S/N contrast for the MRR of the work and the tool were obtained as shown in Figs. 3–6. By observing these figures, the significant parameters and their levels were determined as follows:

$$\begin{aligned}&\text{MRR of work} : I_{\mathrm{p}} : 3, \mathrm{PL} : +, \mathrm{An} : 2, \mathrm{Ca} : 2, \mathrm{ON} : 2,\\ &\text{Tool wear} : I_{\mathrm{p}} : 1, \mathrm{An} : 3, \mathrm{ON} : 3, \mathrm{SV} : 3, \mathrm{Ca} : 1, \mathrm{PL} : -\end{aligned} \tag{3}$$

Although the levels between the MRR of the work and the tool are different in Eq. (3), the factors are essentially the same. The factors, such as I_{p}, An, Ca and ON, are both non-linear and important in the two cases. From the observations in Fig. 6, the effects of parameter SV (servo standard voltage) on the tool is far less than the effects of I_{p} and An, but close to the effects of Ca and PL. Therefore, SV is a secondary parameter and was not selected. For simplicity, five factors including peak current (I_{p}), polarity of tool (PL), tool (An) and work (Ca) materials, and discharge time (ON) were selected as the most important parameters for both the MMR of the work and the tool.

2.6. PL and ON interaction analysis

The $L_{18}(2^1 \cdot 3^7)$ orthogonal array provides the interaction analysis of columns 1 and 2 without having the effects of

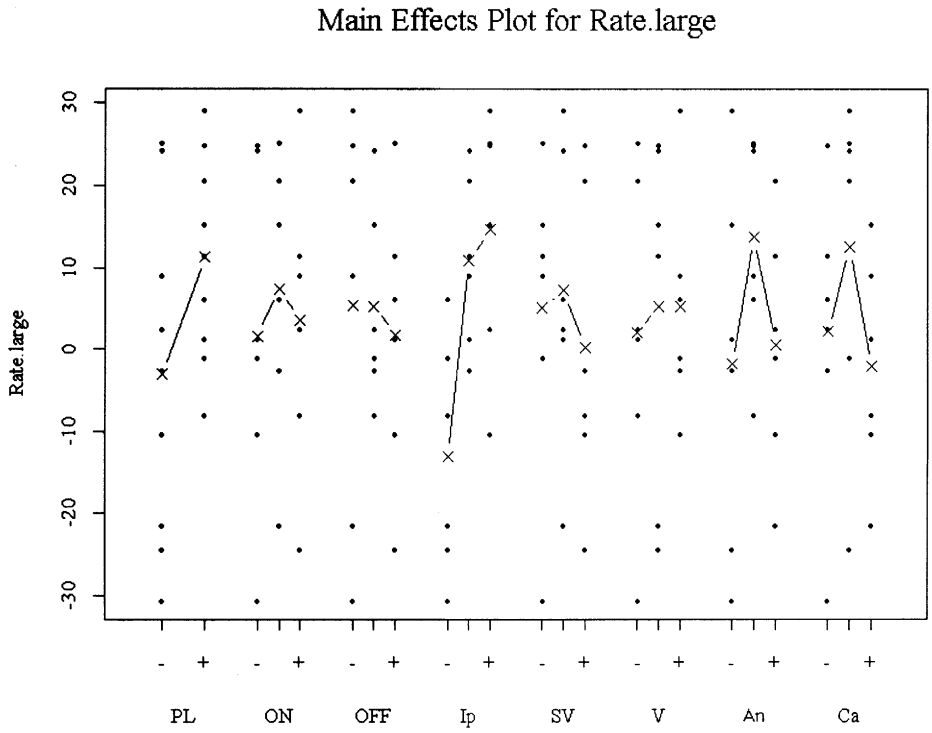

Fig. 3. Response plot for the S/N ratio on the MRR of the work; where control factors and levels are on the abscissa and the S/N value (dB) is the ordinate.

the interactions onto a specific column. Therefore, the plots of interactions between PL and ON on both MRR of work and tool are shown in Figs. 7 and 8, respectively. From the plots, it is noted that PL and ON show no significant interaction.

2.7. Confirmation of important parameters

The response surface method is a collection of statistical and mathematical techniques employed for developing, improving and optimizing an unknown process. In this

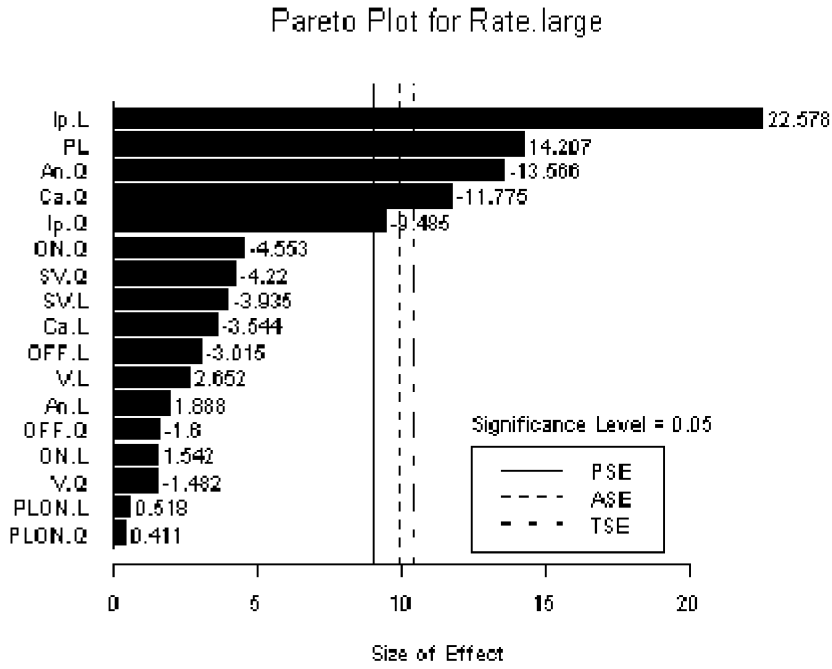

Fig. 4. Pareto plot of factors on the MRR of the work; where the size of effects is the abscissa and the S/N ratio contrast value (dB) is the ordinate.

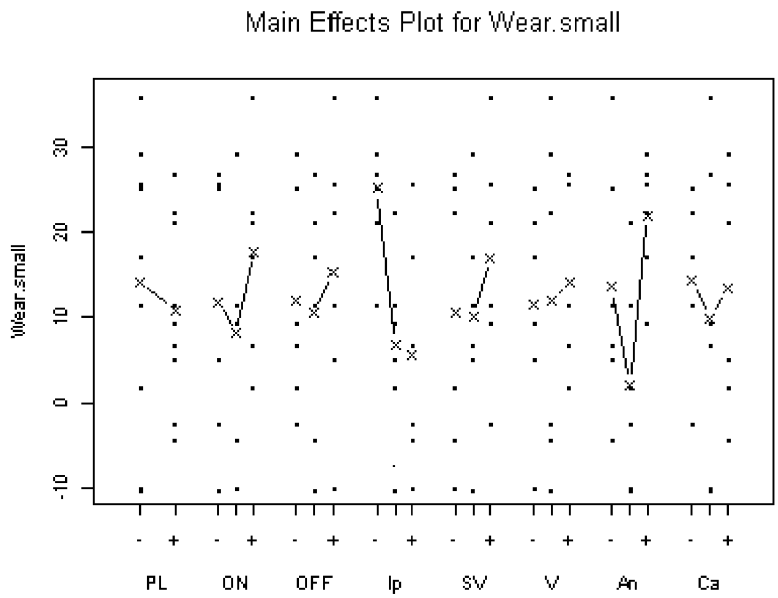

Fig. 5. Response plot for the S/N ratio on tool wear; where control factors and levels are on the abscissa and the S/N value (dB) is the ordinate.

paper, the methodology is used to confirm that the important parameters are steepest ascent points. The factors of ON and I_p were used because they are the most important effects from previous results. The levels of ON and I_p with composite center design of two factors on the MRR of the work are listed in Table 8. The corresponding results are shown in Fig. 9. Although the MRR values of points F, H, I, J, L and M are larger than the value of the central point E (optimal working conditions), these points are not good conditions because the arcing phenomenon was observed. Therefore, the main parameters on the MRR of the work obtained by the Taguchi method are valid. The same results on tool wear were observed when the response surface method was applied with different levels but with the same factors.

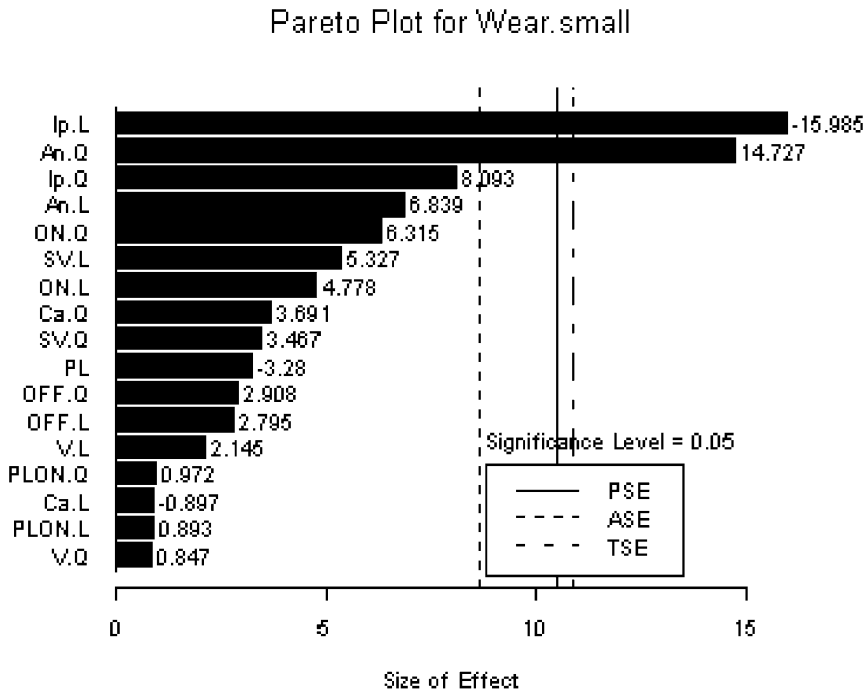

Fig. 6. Pareto plot of factors on tool wear; where the size of effects is the abscissa and the S/N ratio contrast value (dB) is the ordinate.

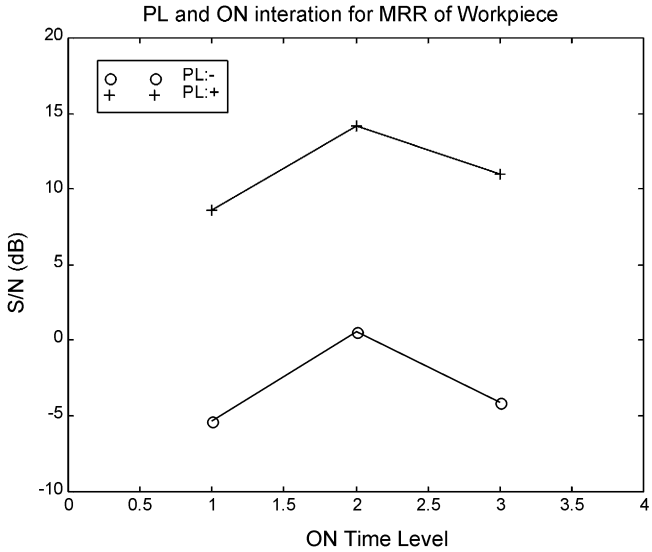

Fig. 7. Plots of PL and ON interactions on the MRR of the work.

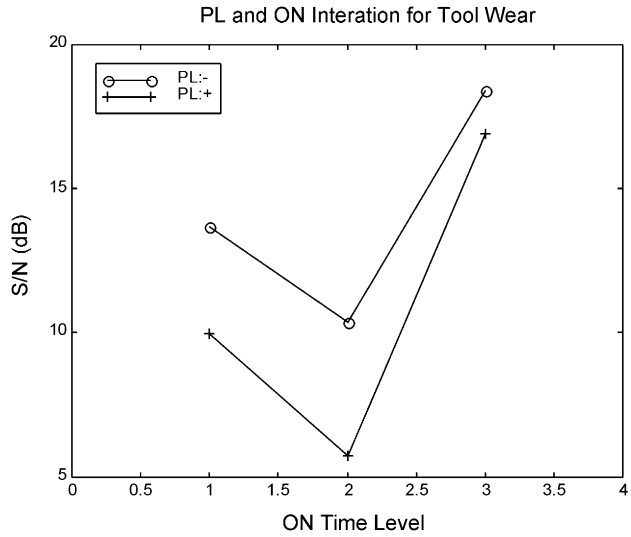

Fig. 8. Plots of PL and ON interactions on tool wear.

Table 8
Central composite design and results of ON and I_p

Run	Factor level		MRR of workpiece (mm^3/min)
	ON (μs)	I_p (A)	
1	20	44	14.411
2	20	52	17.115
3	40	44	24.815
4	40	52	25.327
5	10	48	5.137
6	60	48	24.529
7	30	28	12.469
8	30	68	20.054
9	30	48	19.589
10	30	48	19.764
11	30	48	19.686

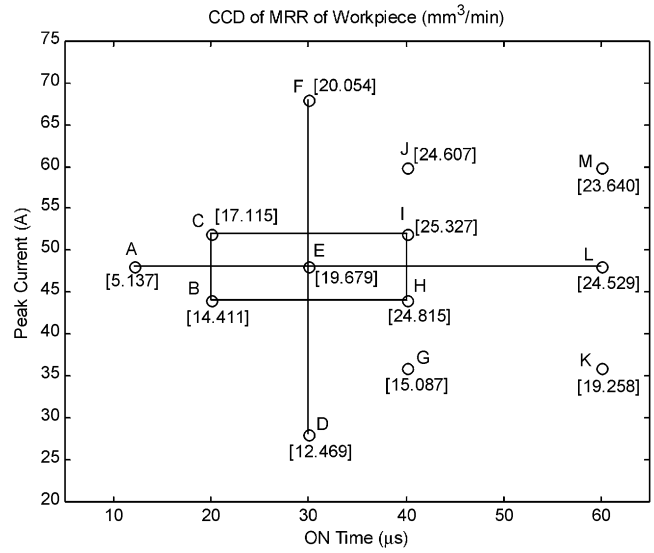

Fig. 9. Experimental results on the MRR of the work by the use of composite center design.

3. Dimensional analysis

The Buckingham $\prod$ theorem states that it is possible to assemble all variables appearing in a problem into a number of dimensionless products (π_i). The required relations connecting the individual variables are determined as algebraic expressions relating the π_i [7,23]. It is noted that the main significant factors have been identified with the help of screening experiments. The optimal process conditions and levels on the MRR of the work and tool are shown in Eq. (3).

According to the breakdown mechanism of short arc discharge, the dissipated energy in the cathode depends on the ionization voltage, cathode drop and work function of the cathode materials. On the contrary, the energy input to the anode depends on the anode voltage drop and the work function of the anode materials [2,24,25]. The effects of the electric polarity on electrode erosion can therefore be expressed in terms of the work function, the ionization potential and the cathode/anode fall either from the viewpoint of the cathode or the anode. As a result, the physical and thermal properties of the materials employed in this study are described as follows:

1. work function (f);
2. input energy of electrode (E)

$$E \propto V_i + V_c - \varphi \text{ when material in the cathode}$$
$$E \propto V_a + \varphi \text{ when material in the anode}$$

where V_i is the ionization energy, V_c the cathode fall, V_a the anode fall, φ is work function;
3. specific heat capacity (C_p);
4. density (ρ);
5. electric conductivity (σ);

Table 9
Dimensions of important parameters in EDM process

	Factor	Symbol	Unit	Dimension (MKSA)
Quality characteristic	MRR of electrode	$\dot{V}$	mm^3/min	L^3T^{-1}
Parameter	Discharge time	τ_{ON}	μs	T
	Peak current	I_p	A	I
	Polarity	PL	–	1
	Input energy onto electrode	E	cal/s	ML^2T^{-3}
Material	Density	ρ	g/cm^3	ML^{-3}
	Electrical conductivity	σ	$(\Omega^a\ cm)^{-1}$	$M^{-1}L^{-3}T^3I^2$
	Specific heat capacity	C_p	cal/(s mol °C)	$L^2T^{-2}\theta^{-1}$
	Thermal conductivity	κ	cal/(mol °C)	$MLT^{-3}\theta^{-1}$
	Melting point	T_m	°C	θ
	Boiling point	T_v	°C	θ
	Latent heat of fusion per unit mass	H_m	cal/g	L^2T^{-2}
	Latent heat of vapor per unit mass	H_v	cal/g	L^2T^{-2}

[a] $\Omega = V/A = m^2\,kg\,S^{-3}\,A^{-2}$.

6. thermal conductivity (κ);
7. melting point (T_m) and vapor point (T_v);
8. latent heat of fusion (H_m) and latent heat of evaporation (H_v).

Table 9 shows the representative dimensions of the above eight properties.

From the parameters mentioned in previous sections, the relationship of the MRR of the work/tool can be expressed as follows:

$$\dot{V} = f(I_p, \tau_{ON}, E, T_m, T_v, \sigma, C_p, \kappa, \rho, H_m, H_v). \quad (4)$$

For most of the metals, it is noted that the value of H_m is approximately equal to $\frac{1}{15}H_v$ [5]. From theoretical conjecture in the EDM process, the work metal is removed essentially by evaporation but a small amount of molten metal remains in the crater. Part of the crater may be ejected owing to the various forces operating in the spark region based on observations in the past [5]. Therefore, it seems justified to neglect the effects of the latent heat and the melting temperature. Now, Eq. (4) reduces to the following:

$$\dot{V} = f(I_p, \tau_{ON}, E, T_v, \sigma, C_p, \kappa, \rho, H_v). \quad (5)$$

Since the dimensionless homogeneous equation of quality characteristics have 10 variables and only five fundamental dimensionless parts, the solution can be expressed in the form of a product of five independent dimensionless part π_s. According to the Buckingham $\prod$ theorem, the dimensional formula on both the MRR of the work and the tool can now be written as

$$c[L^3T^{-1}]^a[I]^b[T]^c[ML^2T^{-3}]^d[\theta]^e[M^{-1}L^{-3}T^3I^2]^f[L^2T^{-2}\theta^{-1}]^g \times [MLT^{-3}\theta^{-1}]^h[ML^{-3}]^i[L^2T^{-2}]^j = [M^0L^0T^0\theta^0I^0]. \quad (6)$$

By equating the powers of the fundamental units on both sides of Eq. (6), a set of simultaneous linear equations are obtained and solved for some constants with detailed derivations given in Appendix A. The equation on the MRR of the work (or tool wear) is given as

$$\dot{V} = A_1\left[\frac{\alpha^2}{H_v^{1/2}}\right]\left(\frac{I_p}{\sigma^{1/2}\rho^{1/2}\alpha^{3/2}}\right)^{a_1}\left(\frac{\tau_{ON}H_v}{\alpha}\right)^{b_1} \times \left(\frac{E}{\rho\alpha^2H_v^{1/2}}\right)^{c_1}(J_a)^{d_1}, \quad (7)$$

where a_1, b_1, c_1 and d_1 are the power index of the corresponding dimensionless brackets in Eq. (7). It should be noted that the thermal diffusivity α of the materials appears with different power index in all the brackets except for J_a.

4. Results and discussion

The semi-empirical model on the MRR of the work and the tool has been shown in the previous section consisting of basic parameters such as peak current, pulse duration, electric polarity and the properties of materials. A series of experiments have been conducted for verification of the semi-empirical model on various combinations of work and tool materials. The parameters and levels of the verification experiments are listed in Table 5.

Based on the experimental results, the coefficients and the power indexes in Eq. (7) have been calculated for each work and tool material by employing linear or non-linear regression analysis. In the linear analysis, the least-squares method is adequate for this study, and in non-linear analysis, four methods, namely the Gauss–Newton, the Davidon–Fletcher–Powell (DFP), the Broyden–Fletcher–Goldfarb–Shanno (BFGS), and the Simplex method, have been adopted for this study. In the DFP and BFGS methods, cubic and mixed cubic/quadratic polynomial line search methods were used for the search direction, respectively [26,27]. In Table 10, an example of the final results on the model with copper as the tool and aluminum and iron as the

Table 10
The coefficients and indexes of the model on the MRR

Optimization method	Linear model coefficient	*P*-value	Tool: Cu, work: Al, Fe					
			Gauss–Newton	DFP (cubic)	DFP (mixed polynomial)	BFGS (cubic)	BFGS (mixed polynomial)	Simplex
Error tolerance of objection function			1×10^{-20}	1×10^{-5}	1×10^{-5}	1×10^{-5}	1×10^{-5}	1×10^{-7}
Run time (s)			2.58	4.12	5.27	3.19	4.45	39.22
Epochs			791	59	122	45	105	120
RMSE*			2.47894	2.47894	2.47894	2.47894	2.47894	2.47894
R^2	0.8374 (logistic)		0.950303	0.950303	0.950303	0.950303	0.950303	0.950303
A_1	$e^{-510.476}$	0.0000	$e^{-399.235}$	$e^{-399.235}$	$e^{-399.235}$	$e^{-399.235}$	$e^{-399.235}$	$e^{-399.235}$
a_1	1.61587	0.0000	1.69773	1.69773	1.69773	1.69773	1.69773	1.69773
b_1	0.70924	0.0000	0.887267	0.887267	0.887267	0.887267	0.887267	0.887267
c_1	2.18111	0.0000	1.73795	1.73795	1.73795	1.73795	1.73795	1.73795
d_1	−347.736	0.0000	−274.137	−274.137	−274.137	−274.137	−274.137	−274.137

* RMSE : Root Mean Square Error.

work is shown. Also, comparisons on the convergence and effectiveness for the various data-fitting methods are illustrated. Although the R^2 of the linear analysis seems to be good, the final model turned out to be a poor model after the results of residual analysis were verified. It should be noted that the coefficients and the power indexes in the example are consistent for the various data-fitting methods. Also, the Gauss–Newton method has the fastest convergence, but the Simplex method has the best stability.

As mentioned in the literature, the Jacob number (J_a) represents the ratio of sensible heat to latent heat of phase-change of materials in the EDM process [28,29]. Hence, the Jacob number is presumably very dependent of the properties and the microstructure of the work materials. However, if J_a was intentionally neglected on the model in the above example, the final results became very poor as shown in Table 11. This is because the model on the MRR of the work is evidently dependent on the work materials. Therefore, J_a is not negligible when various work materials are used for constructing the model. Based on more experimental data, the coefficients and indexes on the MRR of the work for various combinations are compared again in Table 12. Similarly, the coefficients and indexes on the MRR of the tool for various combinations are compared in Table 13.

By observing the coefficients and indexes of the models, the a_1, c_1 and d_1 are larger than b_1. This observation confirms the results from the screening experiments that the peak current, electric polarity, and properties of the materials are more important than discharge time on the MRR. It might be noted that the R^2 values of the case H and I in Table 12 and the case O and Q in Table 13 are far from unity. This might be because the erosion behavior of titanium is quite different from that of aluminum and iron not only in the thermal, chemical and physical properties but also in the microstructure. Therefore, these metals cannot be represented by a single set of coefficients and power indexes. This leads to the

Table 11
The coefficients and indexes of the model on the MMR (J_a is neglected)

Optimization method	Linear model coefficient	*P*-value	Tool: Cu, work: Al, Fe					
			Gauss–Newton	DFP (cubic)	DFP (mixed polynomial)	BFGS (cubic)	BFGS (mixed polynomial)	Simplex
Error tolerance of objection function			1×10^{-20}	1×10^{-5}	1×10^{-5}	1×10^{-5}	1×10^{-5}	1×10^{-7}
Run time (s)			1.04	1.98	2.52	2.64	2.2	20.82
Epochs			325	29	59	40	50	701
RMSE			7.63383	7.63383	7.63383	7.63383	7.63383	7.63383
R^2	0.373 (logistic)		0.528713	0.528713	0.528713	0.528713	0.528713	0.528713
A_1	$e^{7.69275}$	0.000	$e^{7.09055}$	$e^{7.09056}$	$e^{7.09055}$	$e^{7.09055}$	$e^{7.09054}$	$e^{7.09055}$
a_1	0.714138	0.004	0.505593	0.505594	0.505591	0.505593	0.505589	0.505593
b_1	0.393373	0.056	0.530775	0.530774	0.530778	0.530775	0.530781	0.530775
c_1	−0.0335369	0.867	0.310352	0.310352	0.310353	0.310352	0.310353	0.310352

Table 12
Comparisons of model on the MRR of the work with more cases

	Case No.								
	A	B	C	D	E	F	G	H	I
Tool	Cu	Cu	Cu	Ag	Cu, Ag	Cu	Cu	Cu	Cu, Ag
Work	Al	Fe	Ti	Ti	Ti	Al, Fe	Al, Fe	Al, Fe, Ti	Al, Fe, Ti
RMSE	2.69934	0.547894	0.521432	0.340615	0.53491	7.97393	2.47894	6.44963	5.81405
R^2	0.960074	0.98975	0.889473	0.9647	0.898851	0.485784	0.950303	0.550731	0.563201
A_1	$e^{2.13957}$	$e^{-37.9329}$	$e^{-21.4911}$	$e^{-19.8935}$	$e^{-20.6264}$	$e^{-18.9122}$	$e^{-399.235}$	$e^{-16.1862}$	$e^{-16.4322}$
a_1	1.73186	1.42738	2.24174	2.46788	2.28935	0.551791	1.69773	0.476878	0.479912
b_1	0.857038	1.14486	0.0445329	−0.197552	−0.0675777	0.573891	0.887267	0.49627	0.491699
c_1	1.54942	4.86155	2.56433	2.4519	2.50216	0.19871	1.73795	0.265953	0.265237
d_1							−274.137	6.11693	6.28056

Table 13
Comparisons of model on the MRR of the tool with more cases

	Case No.							
	J	K	L	M	N	O	P	Q
Tool	Cu	Cu	Cu	Ag	Cu	Cu	Cu, Ag	Cu, Ag
Work	Al	Fe	Ti	Ti	Al, Fe	Al, Fe, Ti	Ti	Al, Fe, Ti
RMSE	0.0644579	0.268199	0.0203158	0.0605288	0.220403	0.600774	0.0650403	0.542846
R^2	0.885023	0.9256	0.948658	0.934795	0.914431	0.122555	0.866359	0.141484
A_1	$e^{19.2651}$	e^{420359}	$e^{14.2663}$	$e^{35.3399}$	$e^{39.8051}$	$e^{22.7275}$	$e^{17.8486}$	$e^{-47.2901}$
a_1	2.03201	2.87861	1.74658	1.98333	2.67163	0.334096	1.92716	0.362958
b_1	−0.274865	0.244921	−0.11451	0.613824	0.216484	0.0456377	0.396231	0.073032
c_1	−1.46158	−4.22571	−1.26669	−4.16719	−4.00136	−2.85718	−3.28636	−2.93263
d_1							−7.96793	−48.1478

conclusion that no single set of coefficients and power indexes exists for various work and tool materials in the EDM process.

In the previous paragraphs, the verifications on the coefficients and the power indexes of the model are shown with promising conclusions. Therefore, it is interesting to look at the comparisons on the MRR of the work and the tool between the experimental results and predictions based on the model. In Figs. 10–13, comparisons on the MRR of the work between the experimental results and the model

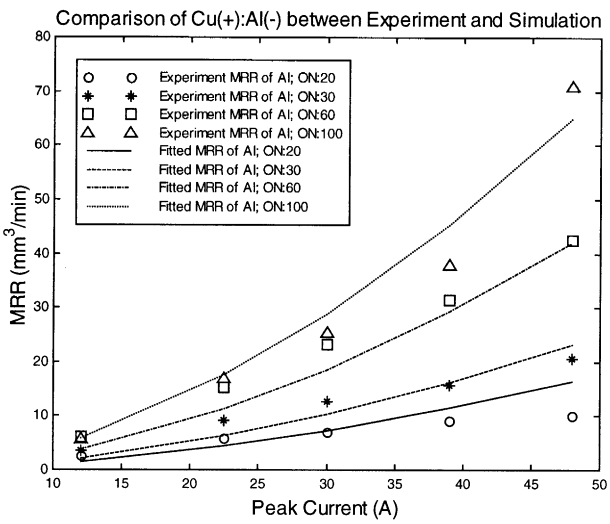

Fig. 10. Comparisons on the MRR of the work between experimental results and model predictions with Al as cathode under the process conditions of case A; tool: Cu(+); work: Al(−); average error = 20%.

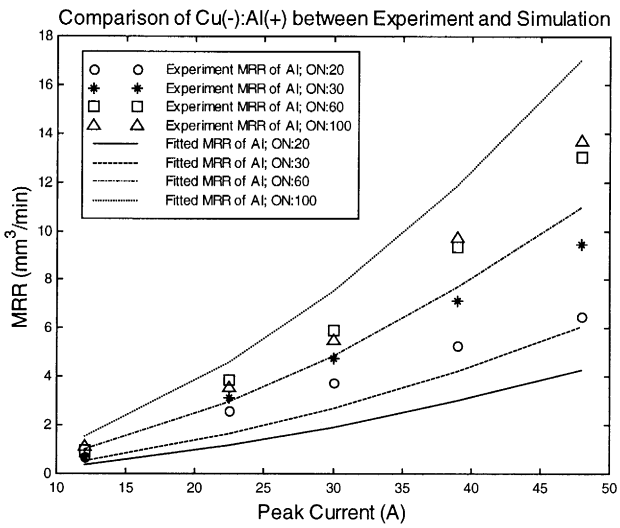

Fig. 11. Comparisons on the MRR of the work between experimental results and model predictions with Al as anode under the process conditions of case A; tool: Cu(−); work: Al(+); average error = 32.41%.

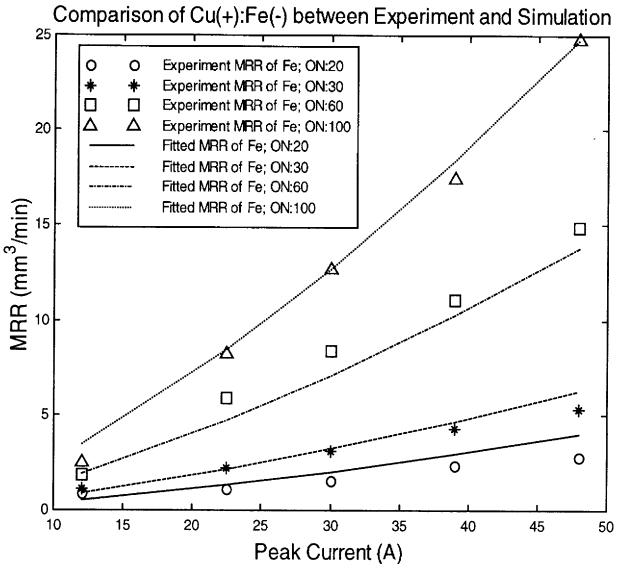

Fig. 12. Comparisons on the MRR of the work between experimental results and model predictions with Fe as cathode under the process conditions of case B; tool: Cu(+); work: Fe(−); average error = 15.74%.

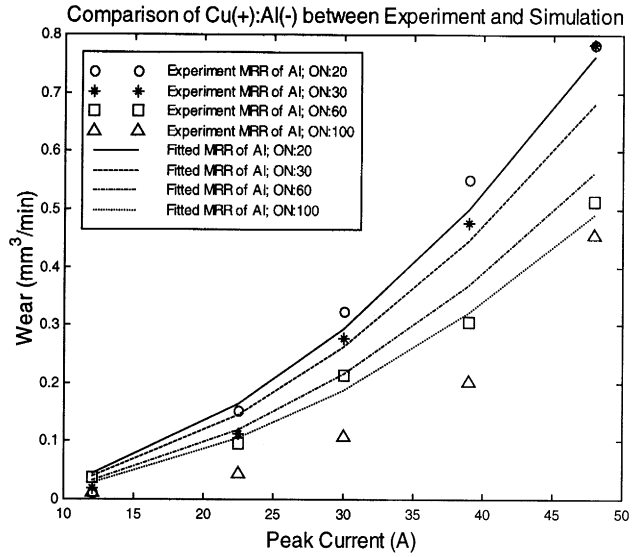

Fig. 14. Comparisons on the MRR of the tool between experimental results and model predictions with Cu as anode under the process conditions of case J; tool: Cu(+); work: Al(−); average error = 50.86%.

predictions are shown with pertinent process parameters. In addition, the comparisons on the MRR of the tool between the experimental results and the model predictions are shown in Figs. 14 and 15 to Figs. 16 and 17 with pertinent process parameters. In these figures, the prediction error is defined as

$$\text{Error}\,(\%) = \left|\frac{\text{Experimental results} - \text{Predictions}}{\text{Experimental results}}\right| \times 100\,(\%). \tag{8}$$

In Figs. 10 and 12, the predictions of the model have errors of less than 20% because the work is the cathode and the MRR is large. It might be noted that the errors on the predictions of the model on the work are smaller than the errors on the predictions of the model on tool wear. By comparing Figs. 14–17, the relations between tool wear and discharge time under different electric polarity are seen to have an inverse effect.

In general, the predictions on the MRR of the work and the tool are in reasonable agreement with the experimental

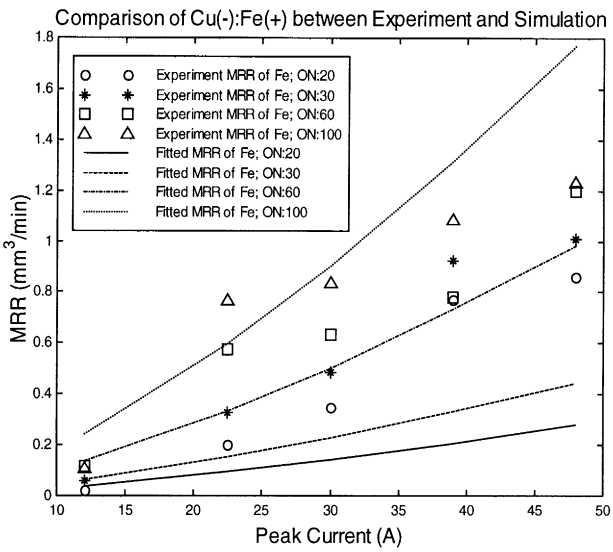

Fig. 13. Comparisons on the MRR of the work between experimental results and model predictions with Fe as cathode under the process conditions of case B; tool: Cu(−); work: Fe(+); average error = 44.29%.

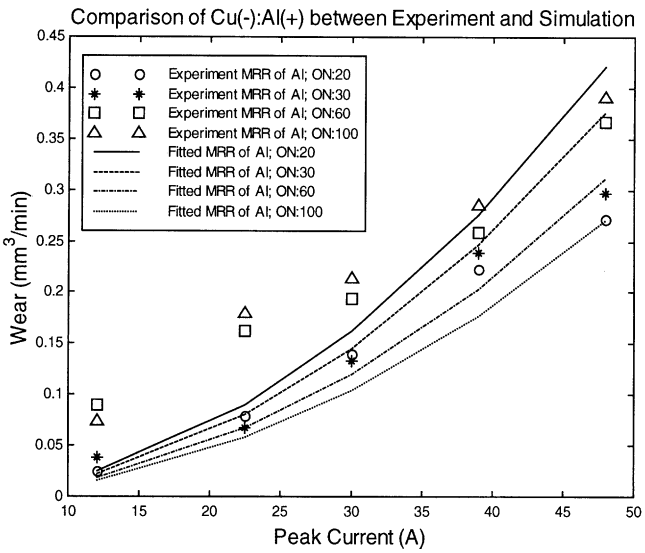

Fig. 15. Comparisons on the MRR of the tool between experimental results and model predictions with Cu as cathode under the process conditions of case J; tool: Cu(−); work: Al(+); average error = 34.49%.

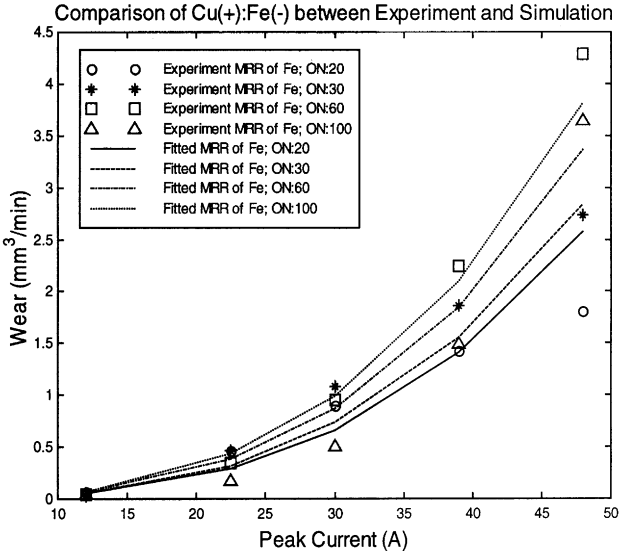

Fig. 16. Comparisons on the MRR of the tool between experimental results and model predictions with Cu as anode under the process conditions of case K; tool: Cu(+); work: Fe(−); average error = 39.96%.

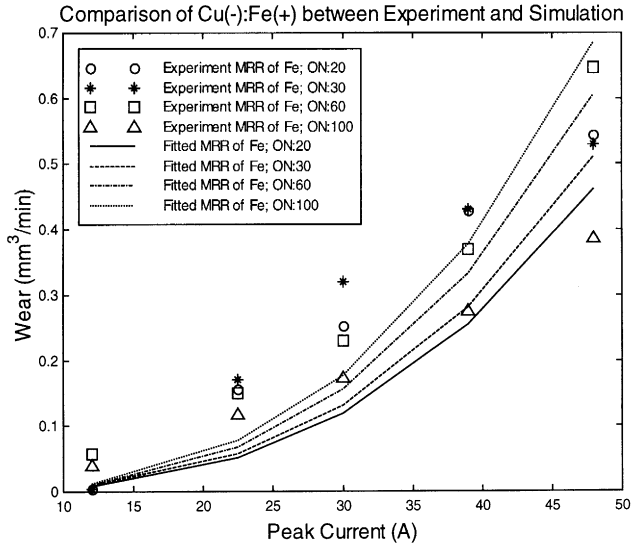

Fig. 17. Comparisons on the MRR of the tool between experimental results and model predictions with Cu as cathode under the process conditions of case K; tool: Cu(−); work: Fe(+); average error = 46.99%.

Table 14
Comparisons of the MRR on the work between experimental data and predictions[a]

	Conditions	MRR on work				
		Workpiece material	Experimental (mm^3/min)	Predictions (mm^3/min)	Differences (mm^3/min)	Error (%)
Model A	Cu(+):Al(−); I_p: 22.5 A, PL: −	Al	17.0111	20.466	3.4549	20.31
Model A	Cu(−):Al(+); I_p: 22.5 A; PL: +	Al	3.2030	5.3668	2.1638	67.56
Model A	Cu(+):Al(−); I_p: 30 A; PL: −	Al	36.797	33.6829	3.1141	8.46
Model A	Cu(−):Al(+); I_p: 30 A; PL: +	Al	8.1402	8.8327	0.6925	8.51
Model B	Cu(+):Fe(−); I_p: 22.5 A; PL: −	Fe	8.399	10.3513	1.9523	23.24
Model B	Cu(−):Fe(+); I_p: 22.5 A; PL: +	Fe	0.5108	0.738	0.2272	44.49
Model B	Cu(+):Fe(−); I_p: 30 A; PL: −	Fe	17.9365	15.6074	2.3291	12.99
Model B	Cu(−):Fe(+); I_p: 30 A; PL: +	Fe	0.9682	1.1128	0.1446	14.94
Model C	Cu(+):Ti(−); I_p: 22.5 A; PL: −	Ti	0.8165	0.9501	0.1336	16.37
Model C	Cu(−):Ti(+); I_p: 22.5 A; PL: +	Ti	0.2929	0.2028	0.0901	30.76
Model C	Cu(+):Ti(−); I_p: 30 A; PL: −	Ti	1.1937	1.8108	0.6171	51.70
Model C	Cu(−):Ti(+); I_p: 30 A; PL: +	Ti	0.9230	0.3865	0.5365	58.13
Model D	Ag(+):Ti(−); I_p: 22.5 A; PL: −	Ti	0.9008	0.7183	0.1825	20.26
Model D	Ag(−):Ti(+); I_p: 22.5 A; PL: +	Ti	0.7855	0.1641	0.6214	79.11

[a] Other conditions for all experiments: τ_{ON}: 120 μs ; τ_{OFF}: 60 μs ; V = 120 V.

verifications. Therefore, more experimental data within the processing window of the screening experiments were measured and employed for further comparisons of the model on the MRR of the work and the tool listed in Tables 14 and 15. In the two tables, although some of the percentage errors in the predictions are large, the actual MRR values are already quite small such that the uncertainties of measurement are already significant for the small MRR measured values. Conclusively speaking, the model works quite well in these verification cases.

5. Conclusions

A semi-empirical model of the material removal rate on the work and the tool in electrical discharge machining has been established by employing dimensional equations based on peak current, pulse duration, electric polarity, and properties of the materials for the screening experiments and the dimensional analysis. The coefficients and power indexes of the model have been data-fitted based on the experimental data generated with the help of the DOE procedure. The final

Table 15
Comparisons of the MRR on the tool between experimental data and predictions[a]

	Conditions	Tool Wear				
		Tool material	Experimental (mm^3/min)	Predictions (mm^3/min)	Differences (mm^3/min)	Error (%)
Model J	Cu(+):Al(−); I_p: 22.5 A; PL: −	Cu	0.0247	0.0998	0.075	303.5
Model J	Cu(−):Al(+); I_p: 22.5 A; PL: +	Cu	0.1304	0.0551	0.0753	57.74
Model J	Cu(+):Al(−); I_p: 30 A; PL: −	Cu	0.3552	0.1790	0.1762	49.61
Model J	Cu(−):Al(+); I_p: 30 A; PL: +	Cu	0.1102	0.0989	0.0113	10.25
Model K	Cu(+):Fe(−); I_p: 22.5 A; PL: −	Cu	0.1214	0.4508	0.3294	271.3
Model K	Cu(−):Fe(+); I_p: 22.5 A; PL: +	Cu	0.0584	0.0810	0.0226	38.60
Model K	Cu(+):Fe(−); I_p: 30 A; PL: −	Cu	0.4878	1.0318	0.5440	111.5
Model K	Cu(−):Fe(+); I_p: 30 A; PL: +	Cu	0.1686	0.1854	0.0168	9.98
Model L	Cu(+):Ti(−); I_p: 22.5 A; PL: −	Cu	0.0202	0.0713	0.0510	252.2
Model L	Cu(−):Ti(+); I_p: 22.5 A; PL: +	Cu	0.0180	0.0426	0.0246	136.8
Model L	Cu(+):Ti(−); I_p: 30 A; PL: −	Cu	0.0922	0.1178	0.0256	27.77
Model L	Cu(−):Ti(+); I_p: 30 A; PL: +	Cu	0.06969	0.0704	0.00071	1.02
Model M	Ag(+):Ti(−); I_p: 22.5 A; PL: −	Ag	0.0953	0.3496	0.2543	266.7
Model M	Ag(−):Ti(+); I_p: 22.5 A; PL: +	Ag	0.0381	0.0964	0.0583	152.9

[a] Other conditions for all experiments: τ_{ON}: 120 μs ; τ_{OFF}: 60 μs ; $V = 120$V.

Table 16
Dimensions of parameters on the MRR of the work and the tool

Dimension	Index (factor)									
	a ($\dot{V}$)	b (I_p)	c (τ_{ON})	D (E)	e (T_v)	f (σ)	g (C_p)	h (κ)	I (ρ)	J (H_v)
M	0	0	0	1	0	−1	0	1	1	0
L	3	0	0	2	0	−3	2	1	−3	2
T	−1	0	1	−3	0	3	−2	−3	0	−2
θ	0	0	0	0	1	0	−1	−1	0	0
I	0	1	0	0	0	2	0	0	0	0

results have indicated that the model is dependent on the materials and therefore cannot be represented by a set of universal coefficients and power indexes for various materials. According to best-fit results from the verification cases, the error analysis shows that the model has reasonable accuracy if the MRR on the work and the tool are large compared to the measurement uncertainties.

Compared to all of the empirical models proposed earlier, the model is mainly based on the thermal, physical, electrical, and material properties of the work and the tool plus pertinent process parameters. Once the coefficients and power indexes of the model have been determined experimentally for given work and tool, the model should be able to give reliable predictions when the process parameters are changed. Of course the model is not based on some fundamental theories, but the potential of this model could be largely explored if the basic phenomena in EDM were better understood.

Appendix A. Derivation of the dimensionless product

The dimensional formula on the MRR of the work and the tool can be written as

$$[\mathrm{L}^3\mathrm{T}^{-1}]^a[\mathrm{I}]^b[\mathrm{T}]^c[\mathrm{ML}^2\mathrm{T}^{-3}]^d[\theta]^e[\mathrm{M}^{-1}\mathrm{L}^{-3}\mathrm{T}^3\mathrm{I}^2]^f[\mathrm{L}^2\mathrm{T}^{-2}\theta^{-1}]^g \times [\mathrm{MLT}^{-3}\theta^{-1}]^h[\mathrm{ML}^{-3}]^i[\mathrm{L}^2\mathrm{T}^{-2}]^j = [\mathrm{M}^0\mathrm{L}^0\mathrm{T}^0\theta^0\mathrm{I}^0] \quad (A.1)$$

By equating the powers of the fundamental units on both sides of Eq. (A.1), a set of simultaneous linear equations are obtained which can later be solved to calculate the magnitudes of these constants. The values of the power indexes on the dimensional parameters are listed in Table 16. Based on the homogeneous linear algebraic equations for the dimensions, the coefficients are the numbers in the rows of the dimensional matrix. The simultaneous equations can be written as

$$\begin{aligned} &d - f + h + i = 0,\\ &3a + 2d - 3f + 2g + h - 3i + 2j = 0,\\ &\quad -a + c - 3d + 3f - 2g - 3h - 2j = 0,\\ &e - g - h = 0, \qquad b + 2f = 0. \end{aligned} \quad (A.2)$$

Now, Eq. (A.2) can be rewritten into a matrix form:

$$AX = C_1, \quad (A.3)$$

where

$$A = \begin{bmatrix} -1 & 0 & 1 & 1 & 0 \\ -3 & 2 & 1 & -3 & 2 \\ 3 & -2 & -3 & 0 & -2 \\ 0 & -1 & -1 & 0 & 0 \\ 2 & 0 & 0 & 0 & 0 \end{bmatrix}, \qquad X = \begin{bmatrix} f \\ g \\ h \\ i \\ j \end{bmatrix}.$$

Solving Eq. (A.3) for five independent dimensionless products gives

1. Assigning $a=1,\ b=c=d=e=0$ gives Eq. (A.3), then
$$C=[0\quad -3\quad 1\quad 0\quad 0]^{\mathrm{T}},$$
$$X=[0\quad 2\quad -2\quad 2\quad \tfrac{1}{2}]^{\mathrm{T}} \tag{A.4}$$
2. Assigning $b=1,\ a=c=d=e=0$ gives Eq. (A.3), then
$$C=[0\quad 0\quad 0\quad 0\quad -1]^{\mathrm{T}},$$
$$X=[-\tfrac{1}{2}\quad \tfrac{3}{2}\quad -\tfrac{3}{2}\quad 1\quad 0]^{\mathrm{T}} \tag{A.5}$$
3. Assigning $c=1,\ a=b=d=e=0$ gives Eq. (A.3), then
$$C=[0\quad 0\quad -1\quad 0\quad 0]^{\mathrm{T}},$$
$$X=[0\quad 1\quad -1\quad 1\quad 1]^{\mathrm{T}} \tag{A.6}$$
4. Assigning $d=1,\ a=b=c=e=0$ gives Eq. (A.3), then
$$C=[-1\quad -2\quad 3\quad 0\quad 0]^{\mathrm{T}},$$
$$X=[\ 0\quad 2\quad -2\quad 1\quad -\tfrac{1}{2}]^{\mathrm{T}} \tag{A.7}$$
5. Assigning $e=1,\ a=b=c=d=0$ gives Eq. (A.3), then
$$C=[0\quad 0\quad 0\quad -1\quad 0]^{\mathrm{T}},$$
$$X=[0\quad 1\quad 0\quad 0\quad -1]^{\mathrm{T}} \tag{A.8}$$

The coefficients of the independent dimensionless products are arranged in Table 17. The complete set of dimensionless products is now rewritten as follows:

$$\pi_1=\frac{\dot{V}C_p^2\rho^2H_{\mathrm{v}}^{1/2}}{\kappa^2}=\frac{\dot{V}H_{\mathrm{v}}^{1/2}}{\alpha^2},$$
$$\pi_2=\frac{I_{\mathrm{p}}C_p^{3/2}\rho}{\sigma^{1/2}\kappa^{3/2}}=\frac{I_{\mathrm{p}}}{\sigma^{1/2}\rho^{1/2}\alpha^{3/2}},$$
$$\pi_3=\frac{\tau_{\mathrm{ON}}C_p\rho H_{\mathrm{v}}}{\kappa}=\frac{\tau_{\mathrm{ON}}H_{\mathrm{v}}}{\alpha},$$
$$\pi_4=\frac{EC_p^2\rho}{\kappa^2H_{\mathrm{v}}^{1/2}}=\frac{E}{\rho\alpha^2H_{\mathrm{v}}^{1/2}},\qquad \pi_5=\frac{T_{\mathrm{v}}C_p}{H_{\mathrm{v}}}=J_{\mathrm{a}} \tag{A.9}$$

Table 17
Results of dimensional analysis

	π_1	p_2	p_3	p_4	p_5
a	1	0	0	0	0
b	0	1	0	0	0
c	0	0	1	0	0
d	0	0	0	1	0
e	0	0	0	0	1
f	0	−0.5	0	0	0
g	2	1.5	1	2	1
h	−2	−1.5	−1	−2	0
i	2	1	1	1	0
j	0.5	0	1	−0.5	−1

It is noted that J_{a} is the Jacob number and $\alpha=\kappa/\rho C_p$ is the thermal diffusivity. The relation between the above dimensionless products can now be equated as

$$\pi_1=f(p_2,p_3,p_4,p_5), \tag{A.10}$$

By substituting (A.9) into (A.10), the complete dimensional equation is as follows:

$$\frac{\dot{V}H_{\mathrm{v}}^{1/2}}{\alpha^2}=A_1\left(\frac{I_{\mathrm{p}}}{\sigma^{1/2}\rho^{1/2}\alpha^{3/2}}\right)^{a_1}\left(\frac{\tau_{\mathrm{ON}}H_{\mathrm{v}}}{\alpha}\right)^{b_1}\left(\frac{E}{\rho\alpha^2H_{\mathrm{v}}^{1/2}}\right)^{c_1}(J_{\mathrm{a}})^{d_1}, \tag{A.11}$$

which can be rewritten as

$$\dot{V}=A_1\left[\frac{\alpha^2}{H_{\mathrm{v}}^{1/2}}\right]\left(\frac{I_{\mathrm{p}}}{\sigma^{1/2}\rho^{1/2}\alpha^{3/2}}\right)^{a_1}\left(\frac{\tau_{\mathrm{ON}}H_{\mathrm{v}}}{\alpha}\right)^{b_1}\times\left(\frac{E}{\rho\alpha^2H_{\mathrm{v}}^{1/2}}\right)^{c_1}(J_{\mathrm{a}})^{d_1}. \tag{A.12}$$

References

[1] A.S. Zingerman, The effect of thermal conductivity upon the electrical erosion of metals, Soviet Phys.-Tech. Phys. 1 (9) (1956) 1945–1958.
[2] F. Van Dijck, Physico-mathematical analysis of the electro-discharge machining process, Ph.D. Thesis, Catholic University of Leuven, 1973.
[3] S.M. Pandit, K.P. Rajurkar, Crater geometry and volume from electro-discharge machined surface profiles by data dependent systems, ASME J. Eng. Ind. B 102 (4) (1980) 289–295.
[4] A. Erden, B. Kaftanoglu, Thermo-mathematical modelling and optimization of energy pulse forms in electric discharge machining (EDM), Int. J. Mach. Tool Des. Res. 21 (1) (1981) 11–22.
[5] J. Longfellow, J.D. Wood, R.B. Palme, The effects of electrode material properties on the wear ratio in spark-machining, J. Inst. Met. 96 (1968) 614–617.
[6] J.E. Greene, J.L. Guerrero-Alvarez, Electro-erosion of metal surfaces, Metall. Trans. 5 (3) (1974) 695–706.
[7] M.L. Jeswani, Dimensional analysis of tool wear in electrical discharge machining, Wear 55 (1979) 153–161.
[8] Osyczka, J. Zimny, J. Zajac, M. Bielut, An approach to identification and multicriterion optimization of EDM process, in: Proceedings of the 23rd International Machine Tool Design and Research Conference, 1982, pp. 291–296.
[9] Iue, Principle of Electric Discharge Machining: Mold Manufacturing Technique, Mihumi Association of Machining Technique, 1983 (in Japanese).
[10] J.H. Zhang, T.C. Lee, W.S. Lau, Study on the electro-discharge machining of a hot pressed aluminum oxide based ceramic, J. Mater. Proc. Technol. 63 (1997) 908–912.
[11] D.C. Montgomery, Design and Analysis of Experiments, 3rd Edition, Wiley, New York, 1991.
[12] G.S. Peace, Taguchi Method: A Hands — On Approach, Addison-Wesley, Reading, MA, 1993.
[13] R.H. Myers, D.C. Montgomery, Response Surface Methodology, Wiley, New York, 1995.
[14] MathSoft, S-PLUS for Windows: User's Manual, MathSoft, Inc., Seattle, 1993.
[15] T. Coleman, M.A. Branch, A. Grace, Optimization Toolbox: For Use with MATLAB — User's Guide, Version 2, The MathWorks, Inc., MA, USA, 1999.

[16] R.A. Williams, Handbook of the Atomic Elements, Philosophical Library, 1970.
[17] D.E. Gray, American Institute of Physics Handbook, McGraw-Hill, New York, 1963.
[18] C. Kittel, Introduction to Solid State Physics, Wiley, New York, 1996.
[19] G.V. Samsonov, Handbook of the Physicochemical Properties of the Elements, Oldbourne Publishers, 1968 (Trans. from Russian).
[20] V.E. Grakov, Cathode fall of an arc discharge in a pure metal. I, Soviet Phys.-Tech. Phys. 12 (2) (1967) 286–292.
[21] H.B. Michaelson, Work functions of the elements, J. Appl. Phys. 21 (6) (1950) 536–540.
[22] A. Von Engel, Ionized Gases, 2nd Edition, Oxford Press, Oxford, 1965.
[23] Sedov, Similarity and Dimensional Methods in Mechanics, 10th Edition, CRC Press, Boca Raton, FL, 1993.
[24] T.H. Lee, T-F theory of electron emission in high-current arc, J. Appl. Phys. 30 (2) (1959) 166–171.
[25] J.D. Cobin, E.E. Burger, Analysis of electrode phenomena in the high-current arc, J. Appl. Phys. 26 (7) (1955) 895–900.
[26] E. Polak, Optimization: algorithms and consistent approximations, Applied Mathematical Sciences, Vol. 124, Springer, New York, 1997.
[27] M.S. Bazaraa, H.D. Sherali, C.M. Shetty, Nonlinear programming: theory and algorithms, Wiley, New York, 1993.
[28] G.S.H. Lock, Latent Heat Transfer: An Introduction to Fundamentals, Oxford University Press, Oxford, 1996.
[29] G.F. Hewitt, G.L. Shires, T.R. Bott, Process Heat Transfer, CRC Press, Boca Raton, FL, 1994.